Biochimica et Biophysica Acta, 773 (1984) 61–73
Elsevier

BBA 72097

WAVE-GUIDE SPECTROSCOPY AND ION TRANSPORT IN PLANAR LIPID BILAYERS

H.P. BRAUN, R. WINTER, F.H. KARG and M.E. MICHEL-BEYERLE

Institut für Physikalische und Theoretische Chemie der Technischen Universität München, Lichtenbergstrasse 4, D 8046 Garching (F.R.G.)

(Received October 24th, 1983)

Key words: Ion transport; Planar lipid bilayer; Wave-guide spectroscopy

The refractive indices of the bilayer-electrolyte system allow the membrane to operate as a light-guide. This system is then able to monitor, optically, the flow of ions across the bilayer. The light is coupled into and decoupled from a spherically bulged bilayer by means of optical, single mode fibers. The light wave travels along the curved bilayer for several millimeters. This light transmission depends critically on the angle of incidence between the fiber axis and the tangent to the film. Three transmission peaks were observed when the angle of incidence was varied between 0° and 90°. The transmitted light intensity can be modulated by the application of an electric potential upon the bilayer. The center peak, with maximum light transmission, appears at an angle of incidence which is defined by the launching geometry. A quadratic field dependence (independent of the polarity) is observed, which originates from changes in the shape of the torus transition region. The transmission of the satellite peaks, which appear just before and after the central peak, can also be modulated by an external potential. This modulation signal reflects a linear dependence on the polarity of the external voltage. The phase of the modulation signal changes its sign at each satellite peak. It is shown that this modulation signal originates from the bimolecular area of the lipid film. We present evidence that this transmission modulation occurs as a result of ion transport through the lipid film. This provides the basis for the use of wave-guide spectroscopy to investigate membrane ionic fluxes.

Introduction

Up to now optical techniques have played a minor role in the investigation of transport phenomena in lipid bilayers. The main shortcoming of normal incidence spectroscopy is the modest path of interaction between the light and lipid film. The recently developed method of wave-guide spectroscopy [1] substantially increases this interaction by coupling a light wave to the bilayer and allows (see below) the use of optical spectroscopy for various membrane phenomena, including ion transport.

In this case, with the light wave propagating in parallel to the surface of the lipid film, the position of the maximum light field is confined within the film, whereas it is exponentially attenuated along a distance of some ten wavelengths within the adjacent electrolyte. Therefore the volume of interaction is not only restricted to the bilayer itself, but extends into the adjacent bulk electrolyte and therefore allows both regions to be interrogated. Since the publication of our first paper concerning wave-guide spectroscopy in lipid films [1], the technique has been considerably refined. Single-mode fibers, with very small numerical aperture, are now available and therefore light waves of zero mode order can now be properly launched, with a small angular spread of its intensity distribution. Provisions have also been made which allow a very precise positioning of the film with respect to the fibers. In the present study we show the existence of different types of guided light waves along the bilayer and then illustrate how they can be used to follow (a) changes in

membrane shape and thickness and (b) ion transport phenomena across the bilayer.

Materials and Methods

Light transmission experiments were made with black lipid films, either from phospholipids or from oxidized cholesterol. These black films were prepared according to the technique of Mueller et al. [2]. The lipids used were solutions of asolectin (Sigma) and dioleoylphosphatidylcholine (Sigma) in *n*-decane (Fluka, puriss.) at a concentration of 2% w/v. Oxidized cholesterol was prepared from cholesterol (Sigma) according to Tien et al. [3]. Various unbuffered aqueous alkali chloride electrolytes (Li, Na, K, Rb) with concentrations ranging from distilled water to 2 M solutions were used for the transmission experiments.

The electrical circuit for charging the bilayer consisted of a triggerable pulse generator with 50 Ω output impedance, giving a bipolar voltage pulse with independent amplitude and time settings for each polarity. The amplitudes and pulse durations were adjusted symmetrically in order to produce no net charge transport during one cycle of the voltage pulse. The current was measured by a current to voltage converter with a sensitivity of 1 V per $1 \cdot 10^{-7}$ A, an effective input resistance of approx. 1 kΩ and a bandwidth of 50 kHz. Ag/AgCl electrodes of area 3 cm^2 were used, giving a path resistance in the electrolyte of 300 Ω with 0.1 M NaCl.

The experimental setup is depicted in Fig. 1A. A typical transmission experiment is shown, where the 514.5 nm emission from an argon cw-laser (Spectra Physics, Model 164) is focussed into single-mode fibers with very small aperture (Siemens AG München, experimental type fiber, numerical aperture approx. 10^{-2}, single-mode operation at 800 nm). The fibers were cut [4] into pieces of 10 cm to 20 cm length and the quality of the endfaces was visually inspected by a microscope. Light modes excited in the cladding were stripped by immersing the fiber in a fluid which has both high optically absorbance and high refractive index. The other end of the fiber is fed through a channel in the separator foil into the circular aperture of 2 mm diameter, where the membrane is formed (Fig. 1B). A similar fiber at

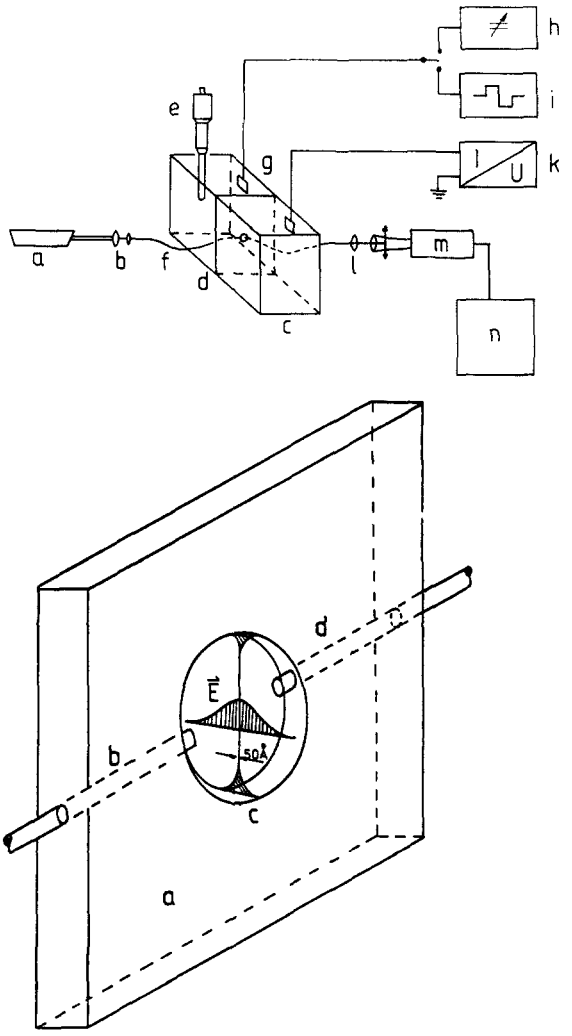

Fig. 1. (A) Scheme of the experimental setup. (a) cw argon ion laser, (b) lenses focussing laser intensity to a single mode optical fiber, (c) electrolyte cell, (d) separator foil containing with circular aperture an input and output fiber, (e) micrometer driven bar for electrolyte adjustment, (f) optical fiber, (g) Ag/AgCl electrodes; an ac capacitance bridge (h) or a pulse generator (i) can be switched to the high-potential electrode. The low-potential electrode is terminated by a current-to-voltage converter (k), (l) polarizer, (m) photomultiplier, (n) signal averager. (B) Scheme of the separator foil. (a) separator sheet, thickness 0.25 mm, polyethylene, (b) channel (40 μm diameter) containing the input fiber, (c) circular aperture (2 mm diameter), (d) output fiber.

the opposite side of the aperture collectes the light from the lipid film. The fibers can be moved within the channels to adjust the angle of inci-

dence with respect to the surface tangent of the film. Normally the black film does not rupture when the fibers are moved.

The light-guide experiments were performed with curved wave-guides. This is necessary to avoid direct interaction between the input and the output fibers, which would swamp the guided intensity with large amounts of directly exchanged light intensity. Thus the fibers are arranged so that the fiber ends and the lipid film form part of a circle.

The angular position of the film with respect to the fiber axis is manipulated by bulging the lipid film. This is achieved by excerting hydrostatic pressure to one of the electrolyte compartments. If two open compartments are used then a micrometer driven bar dipping into the electrolyte will excert a hydrostatic force. However, the open cell arrangement is very sensitive to mechanical noise pickup, which causes irregular oscillations of the lipid film about its equilibrium position. Large fluctuations of the transmitted intensity result since the coupling conditions change with the uncontrolled motion of the film. A significant improvement in the noise level can be achieved by using one closed compartment. In this case the pressure is controlled by a micrometer driven microliter syringe which is attached to the closed compartment.

The condition of the bulged, black lipid film is monitored via its electrical capacitance, assuming that any increase in capacitance is proportional to the increase in bimolecular area. An ac capacitance bridge equipped with a lock-in null detector giving 10^{-5} of relative resolution was used for this purpose.

Fig. 2 shows a cross-sectional view of the separator foil. The angle of incidence θ_i between the fiber axis and the tangent to the surface of the film was derived in the following way. A plane film shows minimum capacitance when $\theta = 0$. The angle θ to the tangent of the film at the rim of the aperture of an arbitrarily bulged film (with respect to the plane film) is calculated from the relationship

$$C(\theta)/C(\theta = 0) = 2/(1 + \cos\theta) \qquad (1)$$

Maximum light transmission should occur at optimum coupling conditions, if the light is launched

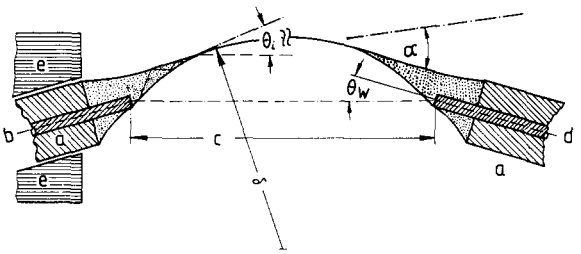

Fig. 2. Cross sectional view of the separator foil. (a) separator foil (polyethylene), (b) optical input fiber, (c) distance between the fibers, (d) output fiber, (e) wedge supports, θ_w = wedge angle, ρ = bending radius of the lipid film, θ_i = angle of incidence between fiber axis and the film tangent, α = angles where radiated intensity is observed, details given in Fig. 7.

in a direction which is finally collinear to the surface tangent of the bulged film at the fiber end.

Signal processing was performed with a modified OMA II system (Princeton Applied Research Corp. 1215) where the signal from the photomultiplier (1P28 RCA) was amplified to a voltage of maximal +10 V (PAR 113 PRE-AMP) and fed to the AD-converter of the OMA head controller (PAR 1216). The system works as a signal averager with 13-bit resolution, a minimum conversion time of 20 μs per channel and a maximum number of 3000 channels per frame. The pulse generator is triggered by a divider counter with the beginning of each frame. Typically 100 frames are averaged during one measurement.

Results and Discussion

Characterisation of the various wave-guided modes

Initially we set out to characterize the transmitted waves with respect to their angle of incidence and their longitudinal attenuation along the bilayer. Fig. 3 shows the transmission through the bilayer as a function of the angle of incidence, θ_i, between the fiber axis and the tangent to the surface of the film. The separator foil containing the fibers was mounted between a support wedge, made from PTFE, and its counterpart, with an angle of 150°. Three transmission peaks are observed. The angular spacing between the peaks is 3.5°. The half-transmission points at both sides are separated by an interval of 11°. As the length of the light path along the bilayer is increased so

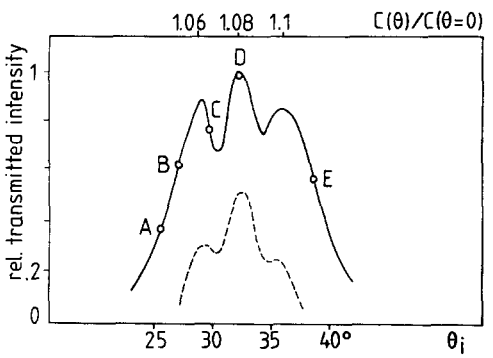

Fig. 3. Light transmission along a black lipid film as a function of the angle of incidence θ_i. Lipid: asolectin in *n*-decane, prepared in a circular aperture of 2 mm diameter, 1 M KCl electrolyte, laser wavelength 514.5 nm. Optical pathlength between the fiber ends: 0.9 mm. The angle of incidence was varied by bulging the bilayer under hydrostatic pressure (injecting an additional volume up to 500 nl into the closed electrolyte compartment). The angles of incidence were derived from the capacitance of the lipid film applying Eqn. 1. The labels A to E refer to the angular positions where subsequent transmission effects were observed. The dashed curve shows the transmission along an optical pathlength of 1.8 mm.

the intensity of the transmitted light decreases. This can be expressed as attenuation coefficient $\mathscr{H}$ in the direction of propagation. $\mathscr{H}$ has been measured by varying the distance between the fibers. The solid curve is measured with a spacing of 0.9 ± 0.1 mm between the fiber ends, while the dotted trace has been recorded at a distance of 1.8 ± 0.1 mm. The field at the center peak shows an attenuation coefficient of $\mathscr{H} = 0.65/\text{mm}$, whereas the lateral peaks propagate with a larger attenuation coefficient of $\mathscr{H} = 1.1/\text{mm}$. The labels A to E in Fig. 3 indicate the angular positions used in the proceeding experiments on the light-intensity modulation.

The light transmission curves recorded for the three types of black lipid film differ in time constants and phase, with respect to the exciting voltage pulse. The influence of the ionic strength of the electrolyte on the shape of the transmission curves is relatively weak. The attenuation of the center peak increases with increasing concentration of the electrolyte. Also the absolute angular position, as well as the spacing between the satellite peaks is changed. These peculiarities will not be discussed in this paper.

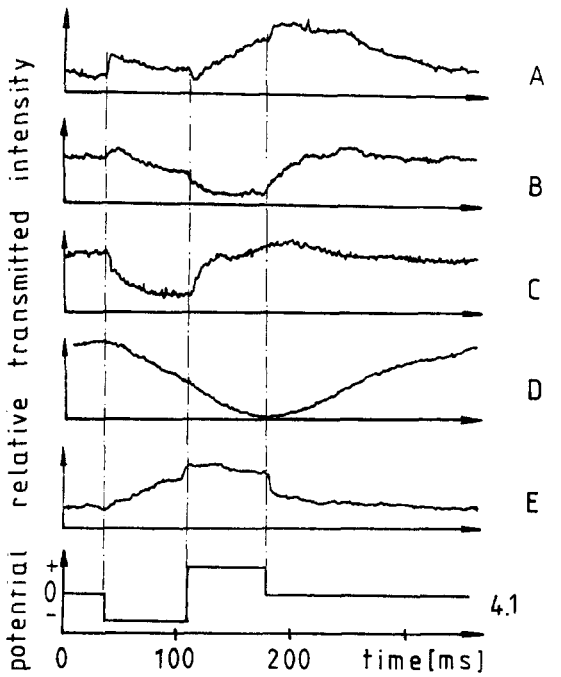

Fig. 4. Modulation of the light transmission by application of an identical voltage pulse. The sequence of time resolved transmission traces was recorded with varying angle of incidence. The bipolar voltage pulse (Fig. 4.1) is totally symmetric in its amplitudes (± 100 mV) and pulse lengths (2×75 ms). The pulse is delayed for 35 ms and its duty cycle is 42%. The field polarity is always referred to the curved outside of the film. Vertical dot-dashed lines illustrate the temporal relation between the exciting voltage pulse and the transmission records. Preparation and geometry are similar to Fig. 3. Fig. 4A was recorded at angular position A ($\theta_i = 25.5°$) in Fig. 3. The transmission at zero potential is defined to be 100%. The fast components of the transmission signal reflect the timing of the exciting voltage pulse. Relative linear intensity modulations of $M_l \approx 5\%$ are observed. This fast signal seems to ride on a slowly varying signal which increases throughout the whole pulse. The change in polarity of the exciting pulse is not reproduced by the slow signal. The quadratic modulation factor is denoted by $M_q \approx 15\%$. Fig. 4B is measured at position B ($\theta_i = 27.0°$). The amplitude of the linear effect increases to 8%, the slow quadratic component is 18%. The trace at position C ($\theta_i = 29.7°$) shows a large linear modulation signal of opposite sign ($M_l = 15\%$). A pure quadratic effect is observed at the maximum position at the center peak, position D ($\theta_i = 32.2°$, $M_q = 42\%$). The linear effect reverses sign at the falling slope of the transmission curve at point E ($\theta_i = 38.6°$).

Figs. 4A–4E show how the intensity of the transmitted light depends upon the angle of incidence at the same external voltage pulse. Time correlation is illustrated by the inclusion of the

exciting voltage pulse (Fig. 4.1). The polarity of the pulse is always related to the outside of the curved film. Black lipid films of asolectin, in 1 M KCl electrolyte, were used.

The 'quadratic effect'

Fig. 4D was recorded at the maximum transmission peak. Even though a bipolar voltage pulse is applied to the film, the transmission signal is independent of the polarity of the applied potential. Voltage dependent capacitance measurements also reveal quadratic relationship between the capacitance and the applied potential. Electrostrictive effects can occur on the shape of the torus and the average thickness of the bilayer or both. These have been discussed in the literature [5–7]. These effects share the common property of a quadratic response to the electric field and they are thus independent of the field polarity. Fig. 5 shows on a magnified scale a light transmission signal (trace a) and the corresponding record of the voltage dependent capacitance (trace b). The slow varying portions of the two signals are similar, but the capacitance trace also shows a more rapid component, which is due to a compression of the average thickness of the black film (microlens compression and orientational effects) [7]. If the bimolecular path of the guided intensity is shortened by moving the fibers together, the slow quadratic modulation signal does not decrease. This indicates that the torus transition region is the origin of the slowly varying modulation.

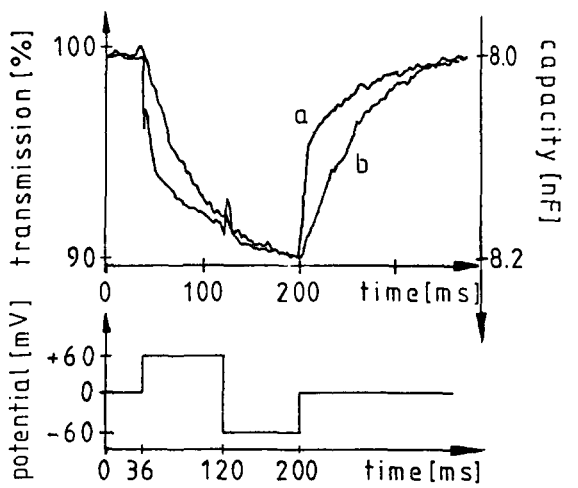

Fig. 5. Comparison between the quadratic effects in light transmission (b) and capacitance (a). Lipid: dioleoylphosphatidylcholine, prepared in 1 M KCl. The light transmission curve was measured in position D. The change in capacity is monitored by the output of the zero voltage detector (phase sensitive detector) from a bridge, balanced at zero volt membrane potential $C(u = 0) = 8.013$ nF. For small changes in capacity the detector output is linear. (In order to achieve a better time resolution the detector output was processed with the signal averager instead of a conventional *RC* low pass integrator).

The torus transition region is defined as that segment of the lipid film, where the thickness of the bilayer decreases from 500 nm along a distance of some 10 μm to the bimolecular thickness of 5 nm [8]. This zone is the most sensitive part to change in shape under the influence of a field induced pressure. In light-guide spectroscopy the transition zone works as a coupler between the light modes of the fiber and those of the bilayer. The coupling efficiency, that is the ratio of light power in the desired mode relatively to the light power in the injected mode, depends critically on the shape of the coupler. Therefore changes in the shape of the transition region are reflected in the coupling efficiency for the zero mode of the fiber into the corresponding zero mode of the planar lipid bilayer. At zero potential the transition zone extends to some 10 μm, depending on the type of lipid, and decreases with increasing potential [8]. A shorter transitions zone reduces its coupling efficiency, thereby scattering more intensity into other directions, than the direction of the mode to be launched into the lipid film. Therefore, electrically induced changes of the shape of the torus transition region can be monitored by simple measurements of transmitted light intensity. A mathematical treatment of the coupling efficiency of a tapered coupler as a function of its geometry is given in [9,10]. The application of the theory of tapered couplers to the torus transition region may help to separate the contribution of voltage dependent capacitance from the contributions of the torus transition and the bilayer region optically. Recent experiments with dioleoylphosphatidylcholine [11], where the observed intensity modulation has been correlated to the change of the contact angle between the bilayer and the torus transition region, were in reasonable agreement to the data of Requena and Haydon [7].

The quadratic effect is always observed, if a

proper wave-guide mode is coupled to the bilayer [1]. Coupling to a proper (surface) mode is best, if the light enters the guiding structure collinearly. In the case of a bent wave-guide the best coupling is where the fiber axis and the surface tangent of the bulged film are collinear. Thus we expect the transmission maximum to occur when the angle of incidence is equal to that of the wedge support. This is true for very small wedge angles. For large angles, however, the transmission maximum is shifted up. With a wedge angle of 15° the transmission maximum appears at 30°. This apparent discrepancy arises from effects in the torus region where the incident beam may be refracted as indicated in Fig. 2.

The deconvolution of the quadratic and the linear effect

In contrast to the quadratic transmission-voltage relation of the center peak, a light transmission with a linear response to the exciting field pulse is observed at the satellite peaks and on their slopes. All the traces A to E in Fig. 4 seem to be the result of the superposition of a linear effect and a quadratic effect. The origin of this quadratic effect is the torus transition region. The reduced coupling efficiency of the torus transition region under external voltage results in an enhanced scattering of light intensity into directions close to that of the electrically undisturbed torus. Since there is no light absorption by the media, an intensity being scattered out of the direction of a proper surface wave must appear elsewhere. Thus outside the centerpeak a quadratic intensity modulation of the opposite sign to that shown in position D is observed. Close to the center peak the quadratic effect is of the same sign as in the center peak; far away from this point the sign of the quadratic contribution changes. With larger angular distance from the maximum transmission point θ_D the quadratic contribution decreases. At the point of widest angular distance (Fig. 4E) the quadratic effect is almost inobservable.

This superposition in a dioleoyl phosphatidylcholine film is illustrated by the sequence depicted in Fig. 6. These curves were recorded at point B in Fig. 3. The first trace was obtained with a polarity of the voltage pulse as depicted in Fig. 6.5. The second trace was recorded with reversed

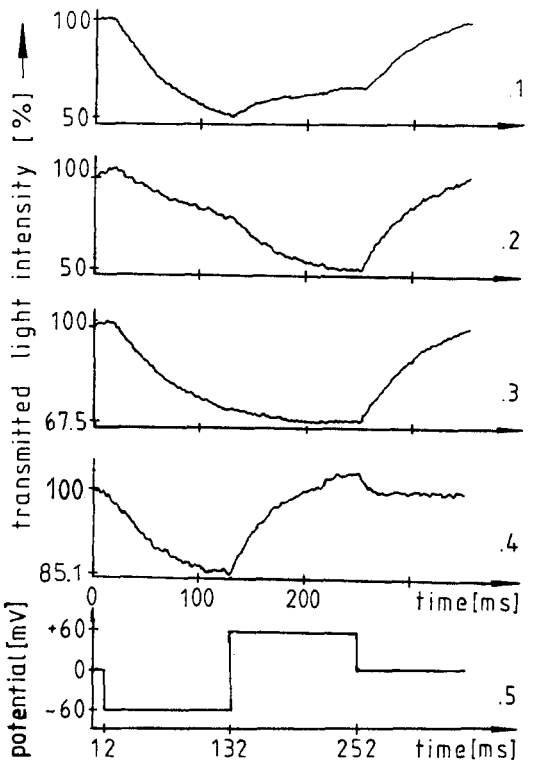

Fig. 6. Deconvolution of the linear and quadratic light transmission effect. Dioleoyl phosphatidylcholine in 0.1 M NaCl, angular position B, bimolecular pathlength 1.2 mm. Fig. 6.1 was recorded with a voltage pulse of the polarity shown in Fig. 6.5. Fig. 6.2 is measured with reversed polarity. Fig. 6.3 shows the average of the proceeding traces, whereas Fig. 6.4 is obtained by subtracting Fig. 6.2 from Fig. 6.1.

polarity. By summing up both traces the linear contributions are canceled and the twice quadratic contributions remains (Fig. 6.3). By subtracting the two traces a linear signal remains which always reflects the change in polarity of the applied voltage (Fig. 6.4). Thus, for a constant angle of incidence the intensity of the transmitted light depends on the polarity of the electric pulse.

An examination of Fig. 6.4 shows a decrease in transmission intensity with the negative polarity outside, but an increase, when the outside is positively charged. The light transmission rises to 105% under the positive potential. The rising and falling slopes of the transmitted intensity show a biphasic time dependence. The fast component of the risetime is 150 ± 20 μs with 5% relative amplitude, while the slow component has a risetime of 37 ± 0.1

ms with 95% relative amplitude. The rise and fall times are very nearly symmetrical. Though the amplitudes of the intensity modulations of the light increase with voltage, the ratios of the relative amplitudes of the two phases are constant.

Finally examining the trace found at the angular position E the linear component of the transmission modulation is of the opposite polarity as observed in position A. All other features remain unchanged.

Transmitted and radiated light intensity

The linear as well as the quadratic effects are observed as modulations of the transmitted intensity. Since there is no light absorption in the lipid or the electrolyte, the light must therefore be radiated out of the direction of propagation of the wave-guide. The following experiment determined the directions where this light intensity was radiated.

A single mode fiber, acting like a photon pickup, was introduced into the electrolyte compartment of the convex bulged film. This fiber was positioned at the same height as the fibers in the separator foil and could be moved at any angle and location with respect to the bilayer. The film was adjusted to an angular position B. A composite linear and quadratic signal was observed with the separator fibers in transmission mode (Fig. 7.2). When the pickup fiber was held in parallel and close to the output fiber (d in Fig. 2) a very distinct linear modulation effect could be detected on the radiated intensity (Fig. 7.1). The phase of this modulation was complementary to the modulation observed in the transmission mode. With successive inclination of the pickup fiber towards the bilayer surface less radiated intensity and modulation of that intensity was detected. The angle α where the modulation of the radiated intensity was detected is indicated in Fig. 2 at the right corner. A value of $5 \pm 2°$ was determined experimentally for α.

The origin of the linear effect

The most interesting question is whether the modulation of the light intensity is controlled by the voltage or by the current. Only if the modulation of the transmitted light is controlled by the current this experimental method will be useful in

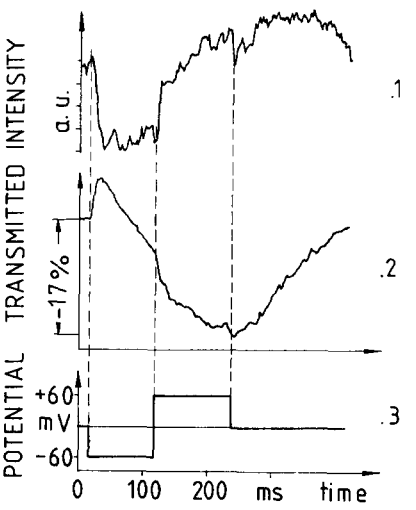

Fig. 7. Signal modulation of the radiated intensity. The intensity being radiated from the bilayer wave-guide was collected by a freely movable single mode fiber. The fiber was mounted in the electrolyte at the same height and close to the position of the output fiber in the separator, but inclined by an angle α. Film: asolectin in 0.1 M KCl. The angular position of the film corresponds to B. Fig. 7.1 shows the intensity modulation detected by the pickup fiber under an angle of inclination $\alpha = 5°$; distance to the output fiber: 0.2 mm. At angles larger than 15°, no modulation could be detected upon the radiated or scattered intensity. Fig. 7.2 demonstrates the transmission signal obtained by the output fiber in the separator.

the study of ion transport across the bilayer. This question can be answered unequivocally when the concentration of the electrolyte is varied drastically. This was achieved by comparing 1 M KCl to distilled water. The path resistance between the electrodes rises from 300 Ω (1 M KCl) to $7 \cdot 10^5$ Ω for distilled water. A time constant for charging the bilayer of about 6 ms resulted from the increased resistance. But this was fast enough to observe the main amplitude of the linear transmission effect. The quadratic effect was always observed, and was used to allow the voltage drop in the electrolyte to be compensated. This was done by increasing the voltage up to a level where the same quadratic field modulation of the transmitted intensity was observed as in the case of a sufficiently conducting electrolyte. Nevertheless only very small linear contributions could be detected after extensive signal averaging.

This experiment clearly shows that the presence of the linear transmission signal depends upon the

salt content of the electrolyte. No voltage dependent dichroic effects could be detected. This is to be expected since the membrane consists of two layers which are mirror images of one another. Any rotation of the light vector due to electrooptic effects in one layer will be compensated by the counter rotation of the other layer. Thus the net dichroic effect will be zero.

The relationship between the linear transmission modulation and the ionic current has been determined (Fig. 8). The angular position corresponds to point B in Fig. 3. Quasi-stationary modulation amplitudes were recorded following the application of the electric potential for 200 ms. These modulation amplitudes were compared to the dc currents flowing through the film using a steady-state current-voltage curve. Within the accessible voltage range being 10 mV (minimum optical signal to be observed), and 100 mV (film rupture) the amplitudes of the transmission modulation are proportional to the dc current. At least for small currents (less than 10^{-7} A/cm^2) there is a linear relationship between the ionic current and the observed linear transmission modulation.

The experimental results presented show, that the current flowing through the bilayer is related to the 'linear' component of the transmission signal. Ion transport across the lipid bilayer is associated with a change of the refractive indices of the wave-guide. This change is monitored by the intensity of the guided light.

A transport induced optical asymmetry in the black film waveguide will occur if either the index of refraction of the cation or the anion is different, or their transport properties (drift and diffusion) are unequal. Different products of ion concentration and specific ionic refractive index result.

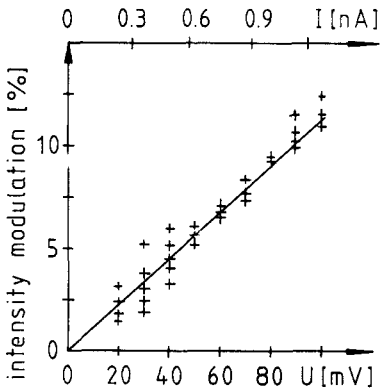

Fig. 8. Intensity modulation versus voltage and current. Film: asolectin in 1 M KCl in angular position B. The amplitudes of the transmission modulations have been plotted versus the exciting voltage pulses and the dc current which would flow under similar permanent voltages.

Principles of wave-guides

A short introduction to the principles of wave-guide optics is now presented to facilitate the discussion of the different wavetypes, which have been experimentally observed.

The wave-guide mode (center peak in Fig. 3)

The electromagnetic field in a wave-guide with a given geometry is fully determined by solving the Maxwell equations with the appropriate boundary conditions [12]. The wave-guide consists of an infinite layer of thickness $2d$ and an index of refraction n_1, surrounded by homogeneous media of refractive index n_2. The analytical expression of the amplitude for the symmetric transverse electric (TE) wave inside and outside the wave-guide is given by (the harmonic oscillations in time and space are omitted):

$$|x| \leq d\colon E_y = A \cdot \cos(ux/d);\ u = 2\pi \cdot (d/\lambda) \cdot \left(n_1^2 - N^2\right)^{1/2} \tag{2a}$$

$$|x| \geq d\colon E_y = A \cdot \cos u \cdot \exp(\pm q \mp qx/d);$$

$$q = 2\pi \cdot (d/\lambda) \cdot \left(N^2 - n_2^2\right)^{1/2} \tag{2b}$$

λ is the vacuum wavelength of the guided light and N is the refractive index of the waveguide in a certain mode. Only TE-modes will be discussed, the transverse magnetic waves are found in the literature being cited. Eqn. 2b describes the transversal attenuation of the wave in the surrounding medium with a characteristic width $w = d/q$.

A description in terms of ray optics with constructively interfering planar waves running in 'zig-zag' mode is equivalent to wave calculations as long as peculiar properties such as the Goos-Hänchen shift at the total reflecting phase boundary are taken into account [13].

Fig. 9 shows the cross-sectional view of a planar

waveguide and the ray path of a bound mode. The prerequisite for wave-guiding, i.e., total reflection, requires that n_1 is always greater than n_2. The light beam enters the guide at A and is reflected at B. The amplitude of the reflected wave is the product of the amplitude of the incident wave times the Fresnel reflection factor R, at B. The reflection coefficient R as a function of the angle of incidence θ_1 is shown in Fig. 10. For angles greater than θ_c we get total reflection. R is a complex number with an absolute value of 1. For θ_1 less than θ_c R is real and less than 1.

$$R_{TE} = (n_1 \cdot \cos\theta_1 - n_2 \cos\theta_2)/(n_1 \cos\theta_1 + n_2 \cos\theta_2) \quad (3a)$$

θ_1 and θ_2 are related by Snell's law of refraction.

$$n_1 \cdot \sin\theta_1 = n_2 \cdot \sin\theta_2 \quad (3b)$$

The critical angle of total reflection is defined by:

$$\sin\theta_c = n_2/n_1 \quad (3c)$$

In the case of total reflection R is complex with an absolute value of 1. The totally reflected beam suffers some phase shift Φ with respect to the incident beam, because the reflected wave penetrates a distance Δx into the less denser material and returns to the phase boundary after a lateral shift of Δz. This is the Goos-Hänchen shift. Another phase shift occurs within the layer, when the light passes under an angle θ_M through the lipid material with an index of refraction n_1. This is simply the optical thickness. Obviously the wave energy is not exclusively confined to the physical thickness $2d$ of the wave-guide but is spread over a lateral distance $2d + 2\Delta x$. This represents the effective thickness of the wave-guide d_{eff}. In the wave picture d_{eff} is equivalent to the sum of $2d/q$ plus $2d$. Energy may be transported in the z direction, if one reflection cycle along the points A-B-C is a multiple of 2π. This phase match condition leads to the characteristic equation which defines a bound wave-guide mode by counting the number M of nodes of the light field within the geometry of the wave-guide.

$$4 \cdot (2\pi d/\lambda) \cdot n_1 \cos\theta_M - 4 \tan^{-1}(q/u) = 2\pi \cdot M \quad (4)$$

The solution of Eqn. 4 selects the discrete 'zig-zag'

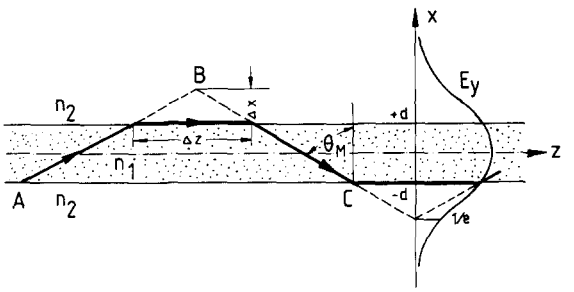

Fig. 9. Ray picture of a light guiding structure. The ray impinges under the angle of propagation, θ_M, of the guided mode at the totally reflecting phase boundary n_1/n_2 ($n_1 > n_2$). It experiences a Goos-Hänchen shift Δz. The right part of the scetch shows the field distribution of the TE mode in the equivalent wave description. Δx corresponds in the ray picture to the $1/e$ point of the transversal attenuated wave. The sum of the physical thickness $2d$ and $2\Delta x$ denotes the effective thickness of the wave-guide.

angle θ_M for a mode. The central and the evanescent parts of the mode travel with a common velocity expressed by a system-index N:

$$N = n_1 \cdot \sin\theta_M \quad (5)$$

Modes of this types are known as surface waves in literature.

The data for the lipid bilayer wave-guide

We can now consider some aspects of a lipid membrane wave-guide. The refractive index of a 1 M KCl electrolyte, n_2, is 1.34 [15]. A commonly accepted value for the refractive index, n_1, of the

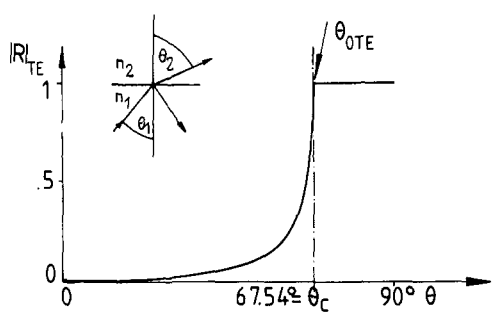

Fig. 10. Reflection coefficient as a function of the angle of incidence. The insert shows the definition of the angle of incidence. For $\theta_1 < \theta_c$ R is real and less than unit. For $\theta_1 > \theta_c$ R is complex and its absolute is unity. The arrow indicates the position of the angle of propagation of the TE surface mode.

lipid film is 1.45 and its physical thickness $2d = 5$ nm is only about 1% of the guided wavelength (using light of $\lambda = 500$ nm) [14]. Therefore only the lowest order mode with the maximum light field centered within the wave-guide can be supported by the film. In this situation the wave-guide index of refraction N is nearly equal to n_2 ($N - n_2 = 4 \cdot 10^{-5}$ for $\lambda = 500$ nm). A further consequence of the small value of the d/λ ratio is a 'zig-zag' angle very close to the critical angle ($\theta_c = 67.53872°$, $\theta_{OTE} = 67.54227°$). Therefore the angular spread of the lossless surface mode must be twice the angular difference $\theta_{OTE} - \theta_c = 0.01°$, otherwise the total reflection condition would be violated. The characteristic length, l, of one reflection cycle between A and C consists of the ray path within the layer and the Goos-Hänchen shifts. It can be calculated as the projection of the ray path onto the surface of the layer. A simple formula (for $\theta_M \approx \theta_c$ with $\theta_M > \theta_c$) is given in Ref. 16.

$$\Delta Z = 2\lambda \cdot \tan\theta_c / \left[2\pi \cdot n_1 \cdot \left(\sin^2\theta_M - \sin^2\theta_c\right)\right] \tag{6}$$

A Goos-Hänchen shift Δz of 86 wavelengths is obtained with both methods. Thus the characteristic length is dominated by the Goos-Hänchen shift. The mode is weakly guided and spreads over a wide transverse distance; the points where the light field decays to a value of $1/e$ are separated by 33 wavelengths. Therefore the plane wave approximations for the description of waveguide phenomena in bilayers are not an over-simplification of the problem.

The radiation loss with a curved wave-guide

The propagation of a surface mode in non absorbing media is virtually without loss. For the sake of simplicity a plane wave-guide has been discussed, but the experiments were performed with spherically curved wave-guides, where unguided light interference can be avoided. The effect of the curvature is discussed below. Another reason for the use of curved guides is that the light wave carried by a planar and symmetric waveguide does not report upon which side a change in refractive index takes place. In order to distinguish sidedness, it is necessary to 'label' one side of the symmetrical wave-guide with respect to its wave-guiding properties by bending the guide. The refractive index, which is experienced by a guided wave at the outside of a curved slab, increases with the radial distance from the slab [17]. The wave portion running at the outside of the curvature has to travel a longer path than the inner portion in order to maintain a phasefront which is perpendicular to the wave-guide axis.

The curvature of the wave-guide introduces radiation losses for the surface wave mode. Energy leaks out continuously from the convex side of a bent guide [18]. An estimation of these losses can also be given on the basis of the ray model.

'In general, when a plane wave is incident upon a curved interface, it is only partially reflected. The transmitted wave in medium 2 appeares to originate at a distance y_{tp} from the curved outside (ρ = bending radius from the curved outside).

$$\theta_i \geq \theta_c : y_{tp} = \rho\left[(\sin\theta_i / \sin\theta_c) - 1\right] \tag{7}$$

$$\theta_i \leq \theta_c : y_{tp} = 0 \tag{8}$$

Thus we can view the apparent origin of the transmitted wave at $y_{tp} > 0$ as a form of electromagnetic tunneling. Tunneling arises because the phase velocity of the (bound) wave in medium 2, parallel to the curved interface, is less than the velocity of a plane wave in medium 2 for $y < y_{tp}$. At the position $y = y_{tp}$ these two velocities become equal and the field disassociates itself from the interface by radiating into space' (quoted from Ref. 18).

The location y_{tp} is identical with that point where the outward refractive index $n(r)$ is equal to N. This will change the real transverse attenuation constant into an imaginary one and the field starts to radiate (Eqn. 2b).

The loss of a single reflection at a curved interface is calculated by the generalized transmission coefficient [18]. It is given by the absolute of the Fresnel transmission factor T in Eqn. 9 multiplied by a curvature factor C in Eqn. 10.

$$T_{TE} = 4\left(\cos^2\theta_c / \cos^2\theta_i - 1\right)^{1/2} \tag{9}$$

In the case where the angle of incidence is close to the angle of total reflection, C is given by:

$$C = \exp\left[-4\pi\rho n_1 \cdot \left(\cos^2\theta_c - \cos^2\theta_i\right)^{3/2} / 3\sin^2\theta_i\right] \tag{10}$$

The total radiation loss at the bend in the wave-guide is calculated by ray tracing at a succession of single reflections at the concave interfaces along the whole guiding structure [19]. If l is the length for one reflection cycle and L the total length of the curved guide, the losses sum up to:

$$\Delta P/P = (1 - T \cdot C)^{L/2l} \tag{11}$$

At the concave curvature there is no tunneling and the Fresnel coefficient for the plane interface is valid. The radiation loss computed by this method is in quite good agreement with calculations made with the help of the WKB method [20]. The radiation loss of the bound TE mode along a black film wave-guide of 1 mm length with 2 mm radius of curvature at 500 nm wavelength is approx. 47%.

The leaky wave (satellite peaks in Fig. 3)

Eqn. 4, which defines a wave-guide mode can also be solved for complex angles of propagation. Admitting those angles, the refractive index of the wave-guide, N, turns out to be complex, too. The imaginary part of N accounts for propagation losses of the guided light intensity. This attenuation, however, is due to the leakage of light energy out of the z direction of the wave-guide geometry; it is not due to the absorptive dissipation of light intensity as commonly associated with a complex index of refraction in optical absorption spectroscopy. The incident rays which constitute the wave-guide modes by constructive interference during one reflection cycle are no longer plane waves with a homogeneous amplitude distribution. The complex component in θ introduces a spatial amplitude attenuation in the x and z direction of the ray. An inhomogeneous wave of this type can be visualized as a spatially confined 'ray bundle'. The direction of energy propagation is no longer in parallel to the wave-guide axis, but occurs under a certain angle with respect to it. If the amplitude distribution of the incident beam is known, the above zig-zag ray picture can be extended to complex rays. A complex reflection coefficient R can be derived by inserting the complex angles θ_1 and θ_2 into Eqn. 3a. The reflected and the transmitted field can be calculated, as well as the characteristic length of one reflection cycle. The longitudinal attenuation of the leaky wave is calculated similar to Eqn. 3a [19]. The complex solutions are outlined in Ref. 21 and a detailed discussion of surface and leaky waves is given in [22,23].

A solution of Eqn. 4 for complex N yields leaky waves which propagate with an angle of $\pm 3.3°$ towards the surfaces of the wave-guide. This is exactly the angular separation of the lateral peaks from the center peak which has been found in Fig. 3. The calculated attenuation coefficient of 0.34/mm is somewhat smaller than the observed one, but curvature losses and radiation due to wave-guide imperfections have not been taken into account.

The origin of the change of the linear intensity modulation

A leaky wave is excited by a spatially confined ray bundle where the beam field is distributed with a small angular spread about the main direction of incidence. This beam can be decomposed, by Fourier optics [24], into a spectral distribution of plane waves. A fraction of partial waves of this bundle will experience partial reflection when it is launched at the angle of the satellite peak. As can be seen from Fig. 10, R is a very sensitive function of θ_1 on approaching θ_c from the real side. In our experiments the angle of incidence θ_i will be fixed but the index of refraction n_2 is changed by the ion transport. Thus the critical angle of total reflection and the angle of mode propagation will change with respect to the fixed angle of incidence. A varying portion of the ray bundle may experience partial or total reflection, depending on which side the refractive index of the electrolyte is increased or reduced by ion transport. At the transition point from partial to total reflection, in closest proximity of $\theta_i \approx \theta_c$, R becomes a steep rising function of n_2. This calculation has to be done for all the partial rays of the bundle. The losses must be weighted and summed up according to their spectral amplitude in the bundle. The characteristic length for one reflection cycle is mainly governed by the Goos-Hänchen shift of the totally reflected partial waves of the incident beam. The attenuation coefficient of the leaky wave is calculated, similar to Ref. 19, as the sum of the reflection losses from partial reflections versus the length of the reflection cycle.

Since there is no phaseshift with partial reflec-

tion, the amplitude of the incident wave will be attenuated to the amplitude of the transmitted wave (transmission loss) within a fraction of one wave length. Thus the partially reflected waves monitor the distribution of the refractive indices in the closest proximity of the phase boundary between electrolyte and lipid film.

There are no reliable data about the ion transport through pure films. The concentration profile of monovalent electrolytes at the phase boundaries of a neutral lipid film has been calculated when the film is charged by an external electrical potential [25,26]. Near the positive phase boundary the concentration of the chloride ions increases and the potassium concentration decreases, while on the other side the ratio of ion concentrations is reversed. This exchange of charges across the bilayer is accompanied with a change in the refractive indices at both sides. The space charge is screened with the Debye-Hückel length towards the infinitely extending electrolyte. The refractive indices are easily calculated by multiplying the net molar ion concentrations at each side with the specific molar refractive index of the ion species.

The specific index of refraction for aqueous solutions of potassium, sodium and chloride ions are derived by comparison of equimolar solutions of chloride electrolytes with small cations like H^+, Li^+ [15]. The specific index is calculated by decomposing the total index of refraction of the solutions into aqueous, cationic and anionic contributions. 1 M Cl^- yield $8.2 \cdot 10^{-3}$, 1 M K^+ or 1 M Na^+ yield $1.4 \cdot 10^{-3}$ of additional refractive index.

The variation of the refractive index at the phase boundary is converted into a modulation of the transmitted light intensity by the loss mechanisms of partial reflection and radiation from bendings in the wave-guide. The change of the refractive index is relatively small, approx. 10^{-7} for a 10^{-3} M NaCl solution, but its effect upon the transmitted light intensity is amplified by multiple reflections along the optical path. The linear modulation signal in Figs. 4 and 6 thus monitor, according to our model, the temporal development of the ionic space charge at the phase boundaries.

The leaky wave and the surface mode differ vastly with respect to their penetration into the electrolyte. Due to total reflection the proper surface mode extends some tens of micrometers into the electrolyte, whereas the partial reflections of the leaky wave take place in the immediate proximity of the phase boundary. 'Leaky-wave' spectroscopy, therefore, enables investigation of immediate border-layer phenomena, with extremely high sensitivity to changes of the refractive index in this layer.

Carrier mediated ion transport in black lipid films has been well described and reliable data on this topic exist [27]. Light transmission experiments were carried out with various carriers. The results which agree with those obtained by electrical methods will be published in the next paper in this series.

Conclusions

Wave-guide spectroscopy on black bimolecular films proves to be a very sensitive technique for the investigation of ion transport. The ions are not detected by their electric charge but by their refractive index. A light wave propagating along the guiding structure senses the variation in refractive index generated by the ion transport. The phase information about the refractive index distribution modulated on the wave is converted into an intensity modulation of the transmitted light by the loss mechanisms of the leaky wave and the radiation loss from the curved wave-guide. The technique is applicable to optically absorbing as well as to non-optically absorbing ions. It is well suited for the investigation of current relaxation experiments at short times, where electrical methods are limited by the capacitive charging spike.

Acknowledgements

Financial support from the Deutsche Forschungsgemeinschaft is gratefully acknowledged. One of the authors, H.P. Braun, wants to express his gratitude to several private sponsors, A., J., R. Braun, M. Süss and F. Kreuzer.

References

1 Braun, H.P., Hermann, R. and Michel-Beyerle, M.E. (1979) Z. Naturforsch. 34a, 1436–1455

2 Mueller, P., Rudin, D.O., Tien, H.T. and Wescott, W.G. (1962) Nature 194, 979–980

3 Tien, H.T., Carbone, S. and Dawidowicz, E.A. (1966) Nature 212, 718–719
4 Khoe, G.D., Kuyt, G. and Luijeldijk, J.A. (1981) Appl. Opt. 20, 707–714
5 White, S.H. (1970) Biophys. J. 10, 1127–1148
6 Wobschall, D. (1972) J. Colloid Interface Sci. 40, 416–423
7 Requena, J. and Haydon, D.A. (1975) J. Colloid Interface Sci. 51, 315–327
8 White, S.H. (1972) Biophys. J. 12, 432–445
9 Marcuse, D. (1971) Bell. Syst. Techn. J. 53, 1379–1394
10 Winn, R.K. and Harris, J.H. (1975) IEEE Trans. Microwave Theory Techn. MTT 23, 92–97
11 Karg, F. (1983) Diploma work, T.U. München Institut für Physikalische Chemie, 8046 Garching, F.R.G.
12 Kapany, N.S. and Burke, J.J. (1972) Optical Waveguides, Academic Press, New York
13 Kogenik, H. and Weber, H.P. (1974) J. Opt. Soc. Am. 64, 174–185
14 Jain, M.K. (1972) The Bimolecular Lipid Membrane, pp. 93–94, Van Nostrand Reinhold, New York
15 Handbook of Chemistry and Physics (1977–1978) 58 Edn., CRC Press, Cleveland, OH
16 Snyder, A.W. and Love, J.D. (1976) Appl. Opt. 15, 236–238
17 Chang, D.C. and Kuester, E.F. (1976) Radio Sci. 11, 449–457
18 Snyder, A.W. and Love, J.H. (1975) IEEE Microwave Theory Tech. MTT 23, 134–141
19 Miyagi, M. and Kawakami, S. (1983) J. Opt. Soc. Am. 73, 486–489
20 Kawakami, S., Miyagi, M. and Nishida, S. (1975) Appl. Opt. 14, 2588–2597
21 Kapany, N.S. and Burke, J.J. (1972) Optical waveguides (Yoh-Han Pao and Kelley, P, eds.), pp. 18–34, Academic Press, New York
22 Tamir, T. (1973) Optik 37, 204–228
23 Tamir, T. (1973) Optik 38, 269–297
24 Tamir, T. and Bertoni, H.L. (1971) J. Opt. Soc. Am. 61, 1397–1413
25 Bruner, L.J. (1967) Biophys. J. 7, 947–972
26 Läuger, P. (1969) Biophys. J. 9, 1150–1159
27 Läuger, P., Benz, R., Stark, G., Bamberg, E., Jordan, P.C., Fahr, A. and Brock, W. (1981) Q. Rev. Biophys. 14, 549–598